

# Development and Characterization of Lycopene Encapsulated Surface-Engineered Pegylated PLGA Nanoparticles for Enhanced Bioavailability and Active Targeted Delivery in Breast Cancer Using MNU-Induced Tumor Model

Ananya Rajkumari <sup>1</sup>, Manjir Sarma Katakai <sup>1</sup>, Paulami Pal <sup>1</sup>, Mohini Singh <sup>1</sup>,  
Bani Kumar Jana <sup>1</sup>, Bhaskar Mazumder <sup>1,\*</sup>

<sup>1</sup> Department of Pharmaceutical Sciences, Dibrugarh University, Dibrugarh-786004, Assam, India;

\* Correspondence: [bhmaz@dibru.ac.in](mailto:bhmaz@dibru.ac.in);

Scopus Author ID 36114212800

Received: 12.08.2023; Accepted: 29.01.2024; Published: 21.07.2024

**Abstract:** The pathogenesis of many physiological conditions and pathophysiological processes, including breast cancer, is governed by oxidative stress, which is a well-known fact. Lycopene is an aliphatic hydrocarbon with effective antioxidant properties and anticancer activity, specifically against breast cancer. The present work aimed to deliver lycopene into breast cancer cells by developing folate-receptor-targeted poly (lactide-co-glycolic acid) (PLGA)-polyethylene glycol (PEG) nanoparticles (NPs). The triple conjugate system (PPF) was fabricated, and NPs were prepared, followed by characterization. The final PPF-NPs have a particle size of  $293.1 \pm 14.6$  nm, PDI of  $0.247 \pm 0.05$ , and Zeta potential of  $-31.9$  mV with  $93.11 \pm 1.09$  % of cumulative percentage *in-vitro* drug release. The NPs have shown cytotoxicity in MCF-7 cells. Flow cytometry and fluorescence imaging have shown the status of the internalization of NPs. *In vivo*, prophylactic and anticancer activity has also been established using an MNU-induced rat tumor model with a 6 mg/kg intravenous dose. The PPF-NPs demonstrate excellent internalization of lycopene in breast cancer cells and suggest significant *In vivo* prophylactic and anticancer efficacy.

**Keywords:** Lycopene; PLGA nanoparticle; surface engineering; folate receptor; breast cancer; targeted drug delivery; MNU-induced rat tumor model; MCF-7; MCF-10A.

© 2024 by the authors. This article is an open-access article distributed under the terms and conditions of the Creative Commons Attribution (CC BY) license (<https://creativecommons.org/licenses/by/4.0/>).

## 1. Introduction

Cancer is the leading cause of death worldwide and is characterized by the appearance of abnormal cells undergoing uncontrolled proliferation. The normal hallmark controlling mechanisms fail to control these cells, leading to cancer development termed carcinogenesis. The progression of carcinogenesis involves several steps comprising initiation, promotion, and progression of deserted cells. As an initiation step, DNA (deoxyribonucleic acid) gets damaged first, followed by the promotion step, which instigates the proliferation of cells into abnormal ones. In the progression step, numerous maneuvers converted these abnormal cells into malignant cells [1,2]. Substantial growth in cancer chemotherapeutics has been observed and noted. However, the fatal adverse effects of conventional cancer chemotherapy still pose the prime challenge of making conventional therapy cumbersome [3,4]. Other challenging issue

related to cancer chemotherapy includes the limited bio-accessibility of anticancer agents. Nanotechnology has established a hope to address these challenging issues, and the emerging novel concepts of site-specific targeting utilizing nanotechnology are becoming resourceful modalities. These nanotechnology-based approaches are favorable and advantageous over conventional chemotherapy [4,5]. During the last few years, significant consideration has been drawn for natural dietary products as they have the potential to hold back cancer and minimize the threat of cancer progression via the mechanism of decreasing oxidative stress [6–9]. It is well known that the pathogenesis of many physiological conditions and pathophysiological processes, including cancer, is governed by oxidative stress [10–12]. Among the 600 identified naturally abundant carotenoids, lycopene is an aliphatic hydrocarbon with effective antioxidant properties and anticancer activity, specifically against breast cancer [13–18]. It has been observed that consumption of lycopene is associated with low-risk chronic diseases like cancer and cardiovascular diseases [18–20]. Many epidemiological studies have also revealed lycopene's anti-carcinogenic and antiatherogenic perspective, primarily attributed to its antioxidant properties. Of all the carotenoids, the singlet oxygen quenching activity of lycopene is the highest, and based upon this assumption, several cell culture studies and numerous animal studies were carried out to ascertain its favorable properties. Regardless of its various therapeutic benefits, the clinical application of lycopene is restricted time and again due to its poor physicochemical properties, such as aqueous solubility and poor oral bioavailability [21–23]. Hence, higher therapeutic doses could only fill the loophole, which is usually challenging for conventional dosage forms. Therefore, to formulate an efficient drug delivery system, designing a novel drug delivery system is essential for which polymeric nanoparticulate drug delivery systems have become very popular. These nanoparticles can target poorly water-soluble or amphiphilic drugs as well as genes in tumor tissues [24,25].

Generally, the tumor lymphatic system is absent, and its vasculature is leaky to macromolecules; hence, it is convenient for preferential delivery of nanoparticles to the tumor through the enhanced permeation and retention (EPR) effect via its blood vessels [26]. Moreover, polymeric NPs could minimize the multidrug resistance via internalization of the drug and reduce its efflux from cells mediated by the P-glycoprotein [27–29]. Despite these, it is of vital significance to design a more precise and active drug delivery system capable of targeting tumors and increasing intracellular uptake of drugs to the tumor site. One such coherent means to achieve this is to utilize the particular association between the receptors on the cancer cell surface and targeting moieties or ligands linked to the polymer backbone [30,31]. A significant increase in site-specific targeting is achieved by some targeting ligands like folate and transferrin [32–35]. Preferentially, folate can increase the therapeutic efficacy of many anticancer drugs [36–38]. In many epithelial malignancies, particularly in gynecological cancers, such as breast, ovarian, and endometrial cancer, folate receptor (FR) is overexpressed [39–41]. Folic acid is essential in the biosynthesis of nucleotide bases and is consumed substantially by malignant tumor cells [42]. Therefore, folic acid can be considered a suitable candidate for targeting anticancer drugs in breast cancer. The receptor-mediated targeted delivery system has the potential to improve the biological performance of bioactive molecules. The principal benefits of receptor-mediated targeted nanoparticles via a targeting ligand like folic acid include higher drug loading capacity, particularly for lipophilic drugs, minimizing dose compared to conventional delivery, and site-specific delivery to the tumor. Hence, it aimed to spotlight the anti-carcinogenic effects of lycopene for specific delivery to breast cancer cells. The work was proposed to incorporate nutraceuticals in an active drug

delivery system, which could further improve its utility. This is because, despite the potential repercussions, delivery of nutraceuticals via nanocarriers is still less researched and developed; henceforth, encouraging results of the present endeavor can unlock a new view in the field of nutraceuticals [43–46]. In this study, a pioneer novel system for the delivery of lycopene is developed using a carrier system comprising PLGA, polyethylene glycol (PEG), and folic acid. It is hypothesized that lycopene delivery into the tumor cells could be sustained through intravenous injection to protect it from rapid degradation.

## 2. Materials and Methods

### 2.1. Materials.

Lycopene was obtained as a gift sample from Alpha Remedies, Ambala, India. PLGA (polylactide: glycolide) and polyethylene glycol bis-amine (PEG-bis-amine) (3KDa) were procured from Sigma Aldrich Pvt Ltd (Mumbai, India). Folic acid (FA), N-hydroxysuccinamide (HNHS), and DCC (dicyclohexylcarbodiimide) were purchased from Hi Media Pvt Ltd (Mumbai, India). All other reagents and solvents were of analytical grades and used as procured.

### 2.2. Methods.

The triple conjugate comprising PLGA (polylactide: glycolide), PEG (polyethylene glycol), and Folic Acid was synthesized as a unique carrier system for lycopene. The carrier and delivery system have been termed as PPF. The PPF conjugate was synthesized as described previously [47]. Briefly, a solution of PLGA (85:15) in dichloromethane (DCM) was prepared, to which DCC and HNHS were added at room temperature under a nitrogen atmosphere for 24 hours to activate the PLGA. Activated PLGA dissolved in DCM was added slowly to PEG-bis-amine in DCM dropwise in the ratio of (1:2) with gentle stirring under a nitrogen atmosphere at room temperature for 12 hours. The resultant solution was precipitated with ice-cold diethyl ether, which was further filtered and dissolved in dimethylsulfoxide (DMSO). After confirmation of synthesis of PLGA-PEG (PP) by both Fourier transform infrared spectroscopy (FTIR) and Nuclear Magnetic Resonance (NMR), we proceeded to synthesize PPF polymer. PP copolymer was dissolved in DMSO, which contained folic acid (FOL) activated with DCC, NHS in the ratio of (2:1:1) at room temperature under a nitrogen atmosphere for 12 hours. Activated FOL and NH<sub>2</sub>-PLGA-PEG-NH<sub>2</sub> were added in the ratio of (1:1) at room temperature under a nitrogen atmosphere for 24 hours. Then 50-100 ml of ice-cold methanol was added, and a precipitate was obtained. The precipitate on the filter was dried by keeping it open overnight at room temperature and dissolved in DCM. The supernatant was dried by keeping it overnight. FTIR and NMR also confirmed the formation of PPF.

#### 2.2.1. Fabrication of nanoparticles.

For the preparation of nanoparticles (NPs), double emulsion solvent evaporation (DESE) was opted, as reported previously. About 10 mg of lycopene was taken, dissolved in 2.5 ml dichloromethane, and kept for solubilization [48,49]. After 20-30 minutes the polymers (PLGA (P)/PLGA-PEG (PP)/PLGA-PEG-FOL (PPF) about 20 mg was dissolved in the drug and dichloromethane solution (drug: polymer ratio of 1: 2). Then for the preparation of the first primary emulsion, 2.5 ml of 1.5 % w/v of polyvinyl alcohol (PVA) was added dropwise and

homogenized at high speed 6,000 rpm for 20-30 minutes until a rich creamy or milky white emulsion was formed. The primary emulsion formed was thus confirmed from the creamy or milky white consistency, and it was added dropwise to 25 ml of 0.5 % w/v PVA to form the secondary emulsion by homogenizing at 18,000 rpm for 20-30 minutes. The formed secondary emulsion was then sonicated for 45 minutes and stirred overnight in a magnetic stirrer to evaporate the organic solvent. Eventually, the formed double emulsion was centrifuged at 5,000 rpm for 5 minutes to discard the large particles formed. Then, the supernatant was centrifuged at 15,000 rpm for 30 minutes to get the required nanoparticles, which were washed thrice with distilled water to remove the surfactant and then freeze-dried. Similarly, other formulations were prepared from PLGA (P), PLGA-PEG (PP), and PLGA-PEG-FOL (PPF) using the same concentration of PVA (1.5 % w/v and 0.5 % w/v) in both primary and secondary emulsion but by increasing the volume of PVA to 5ml and 50 ml in primary emulsion and secondary emulsion respectively.

### 2.2.2. Characterization of nanoparticles.

#### 2.2.2.1. Dynamic light scattering (DLS).

The hydrodynamic diameters specified the average particle size and polydispersity index of prepared NPs. The average particle size and polydispersity index (PDI; the measure of the distribution of nanosized particle population) of each NP dispersion were measured on the day of preparation, after one day and a few months afterward, using dynamic light scattering system (Zetasizer Nano ZS-90, Malvern Instruments Ltd., U.K.), at a scattering angle of 90° and 25°C temperature. Prior to the measurement, samples were examined following 10 times dilution with de-ionized water to an adequate scattering intensity. The zeta potential of the NP dispersions was estimated by measuring the electrophoretic mobility using the same instrument. The pH of the NP dispersions was in the range of 5.5–6.0, and the electrophoretic mobility was determined at a field strength of 20 V/cm. Previous to the measurement of zeta potential, all the samples were adjusted to conductivity 50  $\mu$ S/cm with a 0.9% (w/v) NaCl solution.

#### 2.2.2.2. Scanning electronic microscopy (SEM).

The surface morphological study of the NPs was performed by using a Field Emission-Scanning Electron Microscope (FESEM; Hitachi, Japan). A tiny drop of the NP suspension was placed onto a carbon-coated copper grid and kept for 15 min for drying. Grids were then coated with gold to a thickness of about 300 Å using a sputter coater. All the samples were examined under a FESEM at an accelerated voltage of 10 kV and magnification of 2500 $\times$ .

#### 2.2.2.3. Transmission electronic microscopy (TEM).

The morphology of the prepared NPs was studied using a transmission electron microscope (TEM; JEM CX 100) operating at 200 kV and capable of point-to-point resolution.

#### 2.2.2.4. Drug loading (Percentage of Lycopene incorporated into NPs).

To determine drug loading and entrapment efficiency, an accurately weighed amount of PPF-NPs dissolved in DCM was prepared and assayed spectrophotometrically at 475 nm,

as reported previously. The percentage of drug loading and entrapment efficiency was calculated using the following equations:

$$\text{Drug loading efficiency (\%)} = \frac{\text{Amount of drug present in nanoparticles}}{\text{Amount of drug-loaded nanoparticles}} \times 100 \quad (1)$$

$$\text{Entrapment efficiency (\%)} = \frac{\text{Amount of drug present in nanoparticles}}{\text{The initial amount of drug added}} \times 100 \quad (2)$$

#### 2.2.2.5. *In vitro* release study

For the *in vitro* drug release study, PPF-NPs were dispersed in phosphate buffer solution (PBS) (pH 7.4) and incubated at 37°C in an orbital shaker at 60 rotation/minute and 120 rotation/minute. At estimated time intervals, the sample was centrifuged at 13000 rpm for 10-15 minutes. About 0.5 ml of supernatant was analyzed and replaced with 0.5 ml of fresh phosphate buffer solution (pH 7.4). The incubation was continued till the next sampling, and the process continued for 7 days. The process was repeated thrice [50,51].

#### 2.2.3. Cell culture experiments.

##### 2.2.3.1. Cell culture.

MCF-7 (A breast cancer cell line), MCF-10A (Normal human mammary epithelial cell line), and WBC cell line were arranged from the National Centre for Cell Science (Pune, India) by the Department of Pharmaceutical Sciences (Dibrugarh University, India). MCF-7 and MCF-10A cell lines were grown in Dulbecco's Modified Eagle's Medium (DMEM) supplemented with 10% heat-inactivated fetal bovine serum as well as 100 IU/mL penicillin and 100 µg/mL streptomycin. Cells were maintained in a CO<sub>2</sub> incubator at 37°C under a humidified atmosphere (95% air, 5% CO<sub>2</sub>) to reach 70–80% confluence. Human white blood cells (WBCs) were extracted from a blood sample of a healthy donor using an RBC lysis buffer. WBCs were washed with FBS-free DMEM and adjusted to 1 × 10<sup>4</sup> cells/well for analysis.

##### 2.2.3.2. MTT assay.

The cytotoxicity of Lycopene, PPF-NPs, and blank PPF- NPs on MCF-7, MCF-10A, and WBCs cell lines was determined via the reduction of 3-(4, 5-dimethylthiazol- 2-yl)-2, 5-diphenyl tetrazolium bromide (MTT, Sigma) to Formazan [52–54]. MCF-7 cells were treated by increasing concentrations of either NPs or free lycopene (0, 0.05, 0.5, 1, 5, 10, 50, 100 µM). MCF-10A and WBCs were also treated by NPs or free lycopene at 0, 1, 5, 10, 50, 100, and 200 µM concentrations. Briefly, respective cells were seeded at 5000/well in a flat-bottom 96-well culture plate and incubated with different concentrations (0-1000 µM NPs) of PPF-NPs and free lycopene for 24 h. After removing the media, cells were further incubated with MTT solution (5 mg/ml in PBS) at 37°C, and the untreated cells were used as control. After 3 h of incubation, the supernatant was removed. The cells were further treated with 100 µL of DMSO to dissolve the dark blue crystals of formazan, and the absorbance was measured with an enzyme-linked immunosorbent assay reader at 570 nm. The half-maximal lethal concentration of PPF-NPs or free Lycopene (LD50) was also calculated as the concentration required for 50% inhibition of cell growth compared to untreated cells.

#### 2.2.3.3. Flow cytometry: uptake of PPF-NPs by the breast cancer cells (MCF7).

To qualitatively assess PPF-NPs uptake by MCF7 cells, the fluorescein isothiocyanate (FITC) FITC labeled PPF-NPs were used [55]. The FITC labeled PPF-NPs were incubated with MCF7 cells in 6-well plates (in 2 ml serum-free basic medium/well) for 4 h. After removing the media, the cells were washed with phosphate buffer solution (PBS), trypsinized, centrifuged, and suspended in PBS for flow cytometry analysis (excitation/emission 350/461 nm). The instrument threshold for the negative control sample (untreated MCF7) was set at ~1 % level. The percentage of cells exhibiting FITC-fluorescence beyond this threshold value was calculated as a function of NPs uptake.

Further, in both the presence and absence of folate, the uptake of PPF-NPs was measured. Briefly, MCF-7 cells were pretreated with or without folate (500 nM) overnight and seeded onto a 24-well plate (10,000 cells per well) with Dulbecco's Modified Eagle Medium (DMEM). The FITC-labeled NPs were incubated with MCF-7 cells for 4 h. After several washing steps, the uptake of NPs was analyzed using flow cytometry.

#### 2.2.3.4. Apoptosis: an appraisal of the mechanism of cell death.

To indicate whether the mechanism of cell death is through apoptosis, MCF-7 cells were treated with LD50 values of PPF-NPs. The cellular apoptosis was also inspected using a mixture of acridine orange and ethidium bromide staining methods [56]. Acridine orange/ethidium bromide staining was used to visualize nuclear changes and apoptotic body formation, characteristic of apoptosis. Apoptotic cell death was evaluated using acridine orange and ethidium bromide as fluorescent probes. Briefly, cells treated or not treated with PPF-NPs were trypsinized, centrifuged, pelleted, and stained with 20  $\mu$ L of dye mixture containing 15 mg/mL of acridine orange and 50 mg/mL of ethidium bromide in 1 $\times$  PBS and allowed to stain for 5–10 minutes at room temperature. Thereafter, 2–3 drops of the stained cells were placed on each slide with a coverslip. Photographs were taken at random locations under a Nikon 90i fluorescence microscope equipped with Nikon BR software. Untreated cells were used as the negative control.

#### 2.2.4. Acute and chronic toxicity tests in mouse model.

To study the acute and chronic toxicity of PPF-NPs, thirty-six 5-week-old male BALB/c mice weighing an average of 25 g were selected [57,58]. The routine blood parameters were evaluated to screen the toxicity of the NPs. The experiments were approved by the Institutional Animal Ethics Committee (IAEC approval no: IAEC/DU/80 dated 27.03.2015) and housed at the Central Animal House Facility of Dibrugarh University (Regd No. 1576/go/a/11/CPCSEA dated 17.02.2012).

#### 2.2.5. Inhibition of tumor growth in rat model.

Forty-day-old healthy female Sprague–Dawley rats (S/N Chakraborty Enterprise, Kolkata, West Bengal, India, Reg. No. 1433/TO/D/11/CPCSEA) were kept in solid bottom cages with corncob bedding at 22°C and 50% humidity, with a 12-hour light-dark cycle. The rats were given a rat chow diet and a free approach to water. N-Nitroso-N-methylurea (MNU) was used to induce tumors in rats, and the experiment was performed using the well-known method described previously [59–62]. The body weight and diet consumption of the rats were monitored weekly. A digital caliper measured the tumors' dimensions (length  $\times$  width). The

tumor burden was calculated. The rats were sacrificed by carbon dioxide asphyxiation and skinned after twenty-four weeks. On each rat, a detailed autopsy was performed once tumors were excised. The excised mammary tumors were tracked for location, weight, and dimensions, followed by histological examination.

#### 2.2.5. *In vivo* pharmacokinetic study.

For the *In vivo* pharmacokinetic study, rats were divided into two groups, each consisting of 5 rats. In the tail vein, all the groups I and II animals received single-dose bolus administration of lycopene (6 mg/kg) and PPF-NPs (equivalent to 6 mg/kg of free lycopene). Roughly 0.3 mL of blood samples were withdrawn and collected at different time intervals from the eye by retro-orbital plexus method in tubes containing EDTA and refrigerated [62]. The blood collection was performed under mild anesthesia. After each blood collection, dextrose normal saline (1 mL) was administered orally to the animals to recompense the electrolyte and central compartment volume level. Plasma was separated by subjecting the blood samples to centrifugation at 1000 g for 10 min, followed by the addition of 0.1 mL of trichloroacetic acid (10% w/v) to an equal volume of plasma. The mix was then vortexed for a few minutes, and 5 mL acetonitrile was added. The mix was then again vortexed for 10 minutes, followed by centrifugation at 1000 g for 10 min. Finally, the supernatant was separated by filtration utilizing a 0.22  $\mu\text{m}$  membrane filter and quantified for Lycopene by HPLC. The data were collected and analyzed by a modified Wagner Nelson pharmacokinetic model using Kinetica software, version 5.0 (M/s Thermo Scientific, USA) [62,63].

#### 2.2.6. Statistical analysis.

All the results are the mean  $\pm$  SD of three independent experiments. The significance of differences ( $p < 0.05$ ) between experimental variables was evaluated by a two-tailed Student's test (GraphPad Software Package). The statistical significance was indicated by  $p < 0.05$ .

### 3. Results and Discussion

#### 3.1. Results.

PLGA-PEG conjugate was formed by activating PLGA and its subsequent coupling with PEG-bis amine through DCC and NHS coupling reaction. During activation of PLGA, the terminal  $-\text{COOH}$  group gets reactive and binds with the primary amine group of PEG-bis amine through amide bond formation. The addition of an appropriate quantity of PEG-bis amine at this stage is critical as excess of it facilitates the formation of triblock polymer PLGA-PEG-PLGA. Therefore, this reaction is followed by washing and dialysis against distilled water. In the present investigation, a ratio of (2:1:0.5) of PLGA, DCC, and NHS was found to be appropriate for the activation of PLGA, and a ratio of (1:2) of activated PLGA and PEG-bis amine was found to be appropriate for formation of PLGA-PEG with sufficient yield. The sharp peak at 1626.15 at the spectra, which is absent in the PLGA spectra, indicates the conjugation of PEG-bis amine in the carboxylic group of PLGA (Figure 1).

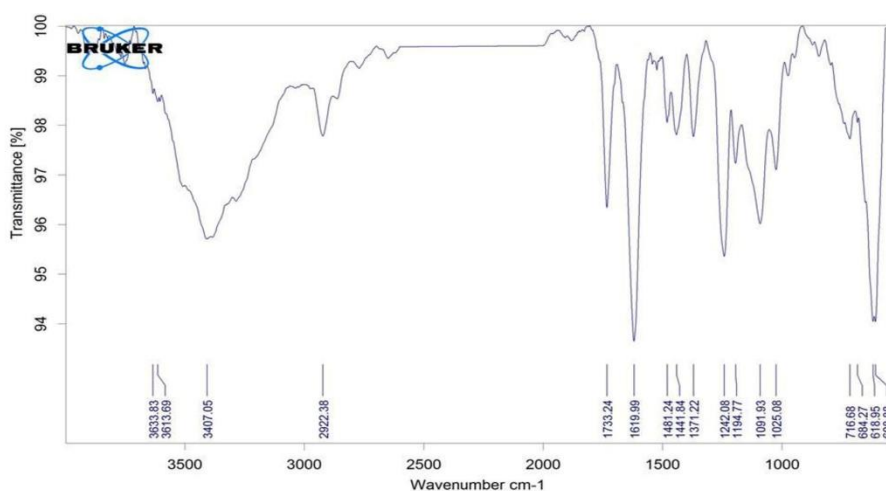


**Figure 1.** FTIR spectra of PPF-NPs.

Peak at 3.6 ppm confirms the conjugation of PEG to PLGA which is due to  $-CH_2$  protons of PEG. Peaks at 1.6 ppm and 5.2 ppm are due to  $-CH_3$  and  $CH$ -protons of PLA of PLGA. At the same time, the peak at 4.8 ppm is due to  $-CH_2-$  protons of PGA of PLGA (Figure 2).

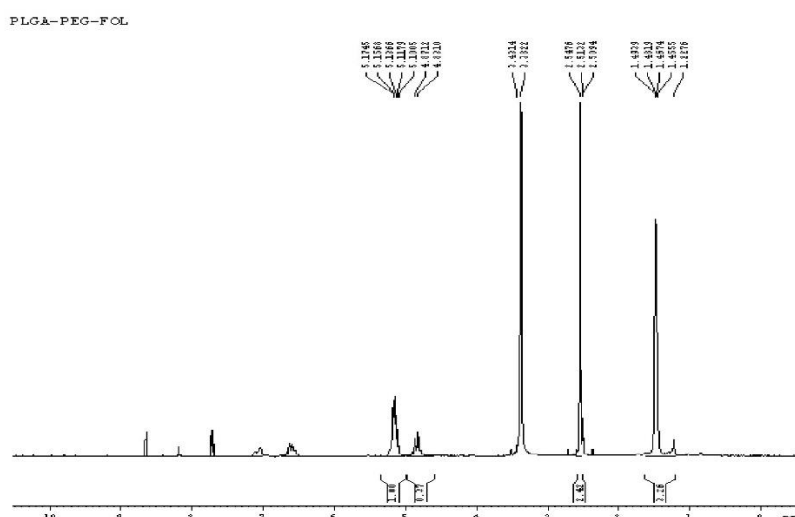


**Figure 2.** NMR spectra of PPF-NPs.

In the present investigation, a ratio of (1:1:2) of DCC, NHS, and Folic acid was used to activate Folic acid. FA has both the carboxylic functional groups  $\alpha$  and  $\gamma$ , and while its activation involves DCC chemistry, both groups can be activated. However, only the  $\gamma$ -carboxylic end group is conjugated to PLGA-PEG as it has higher reactivity.  $NH_2$ -PLGA-PEG- $NH_2$  was then conjugated to activated folic acid by adding in the ratio of (1:1). Formation of PLGA-PEG-Folate was confirmed by FTIR & NMR (Figures 1 and 2). The characteristic peak shown in FTIR of PLGA-PEG-FOL is due to  $-NH$  stretching, carboxylic acid  $C=O$  and  $O-H$  stretching unconjugated and aromatic  $C=C$  bending, respectively. Basically, the conjugation of FA to PLGA-PEG to form PLGA-PEG-FOL is through amide bond formation. This finding is similar to the findings of other studies. A sharp, distinct peak at 1619.99 is due to the  $-CONH-$  group due to the conjugation of PEG from  $-PEG$ -bis amine to PLGA, and stretching vibration between 1619.99 and 1481.24 is because of  $C=C$  stretching of the aromatic ring of FA indicating conjugation of FA to PLGA-PEG (Figure 1). Peaks observed in PLGA-PEG polymer are also found in PLGA-PEG-FOL because of respective protons at PLGA-PEG.

Confirmation of the conjugation of FA to PLGA-PEG to form PLGA-PEG-FOL is due to the presence of small peaks at 6.7, 7, 7.8, and 8.7 ppm (Figure 2). These small peaks are linked with the protons due to folate.

### 3.1.1. Fabrication of PPF-NPs.

Lycopene-loaded NPs were formulated using the DESE method. This method has the potential to obtain formulations with the required characteristics, size, encapsulation, and surface properties. The most critical step in the emulsion technique is the complete emulsification of both the organic and aqueous phases. Although different stabilizers are used, PVA is the most widely used stabilizer. A proper emulsion formation is ensured when a homogeneous, milky white solution is obtained. NPs formation may fail when a broken or poor emulsion with macroscopic heterogeneity or granularity is observed, even with two visually distinct layers. A stable emulsion is attained and maintained by sonication. In the DESE method, when formed particles in primary emulsion are dispersed into larger aqueous volume, the solution should be homogeneously opaque and slightly translucent. When a particle decreases, its translucent quality also increases. Often, blue tint or color may be seen for extremely small particles without a drug. This phenomenon is not observed when the drug is encapsulated within the nanoparticles. The particles formed are dispersed uniformly in the emulsion and re-suspended when vortexed or sonicated in case of failure. The particles obtained after these processes are washed and obtained by centrifugation. When freeze-dried or lyophilized, the particles appear in different textures, varying from cotton-like to free-flowing powder.

### 3.1.2. Characterization of PPF-NPs.

Spherical and smooth surface NPs were observed in SEM images (Figure 3B). The particles loaded with lycopene were in the submicron sizes, which were homogeneously distributed.

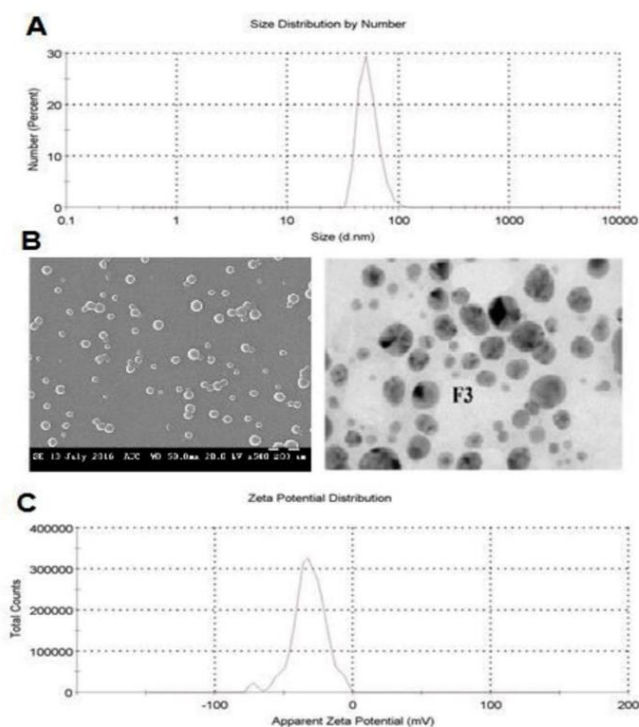


**Figure 3.** (A) Average particle size; (B) SEM and TEM images; (C) Zeta potential of PPF-NPs.

TEM images suggest the drug was distributed in particulate form throughout the NPs body. The release studies of NPs (PPF-NPs) were carried out in PBS (pH 7.4). The cumulative percentage of drugs released was calculated and depicted in Figure 4.

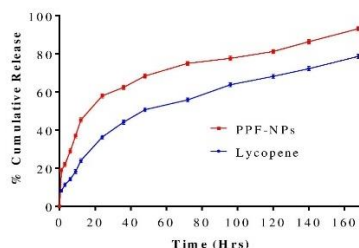


**Figure 4.** In vitro drug release data of Lycopene and PPF-NPs.

From the result of 168 hrs, it was observed that PPF-NPs showed  $93.11 \pm 1.09$  % of cumulative percentage drug release, which is significantly higher than lycopene. The final PPF-NPs have a particle size of  $293.1 \pm 14.6$  nm, a poly-dispersity index of  $0.247 \pm 0.05$ , and a Zeta potential of  $-31.9$  mV (Figure 3A and 3C and Table 1).

**Table 1.** Particle size, polydispersity index, zeta potential, % drug loading, and % entrapment efficiency of PPF-NPs.

Volume and concentration of PVA		Particle Size (nm)	Polydispersity Index (PDI)	Zeta Potential (mV)	Drug Loading (%)	Entrapment Efficiency (%)
		(Mean ± SD)*				
2.5 ml of 1.5 % for primary emulsion	25 ml of 0.5 % for secondary emulsion	$293.1 \pm 14.6$	$0.247 \pm 0.05$	-31.9	$31.667 \pm 0.131$	$72.630 \pm 0.145$
5 ml of 1.5 % for primary emulsion	50 ml of 0.5 % for secondary emulsion	$364.1 \pm 17.4$	$0.572 \pm 0.07$	-28.7	$31.187 \pm 0.162$	$71.083 \pm 0.123$

SEM images of PPF-NPs also showed the nanometric size, spherical shape, and smooth surface of nanoparticles (Figure 3B). PPF-NPs demonstrated higher entrapment efficiency ( $72.630 \pm 0.145$  %) and better drug loading capacity ( $31.667 \pm 0.131$  %) (Table 1). This might be attributed to the higher solubility of lycopene in the synthesized Nanoparticulate system.

### 3.1.3. MTT assay.

An MTT cytotoxicity assay was performed to determine the anti-proliferative effect of Lycopene and PPF-NPs on MCF-7, MCF-10A, and WBCs cell lines. The results showed that PPF-NPs significantly inhibited the proliferation in breast cancer cell lines of MCF-7. However, they did not remarkably affect normal human MCF-10A breast cells and normal WBC (Figure 5).

Lycopene and PPF-NPs induced dose-dependent cytotoxic effects against different cell types. It seems from Table 2 that there is a direct correlation between the toxicity of PPF-NPs and the proliferation rate of treated cells. This may be rationalized in the following way: First, the highest cytotoxicity was seen for the most aggressive cell line with a higher proliferation rate. Second, the cytotoxicity of PPF-NPs against breast cancer cells was much larger (the magnitude of the difference depends on the type of breast cancer cell line) than its cytotoxicity on normal cells. Third, the cytotoxicity of PPF-NPs against breast cancer cells was found to be significantly higher than its cytotoxicity on normal cells (MCF-10A and WBC). Fourth, the trends of LD50 related to PPF-NPs are as follows:  $MCF-7 \ll MCF-10A < WBC$  (Table 2).

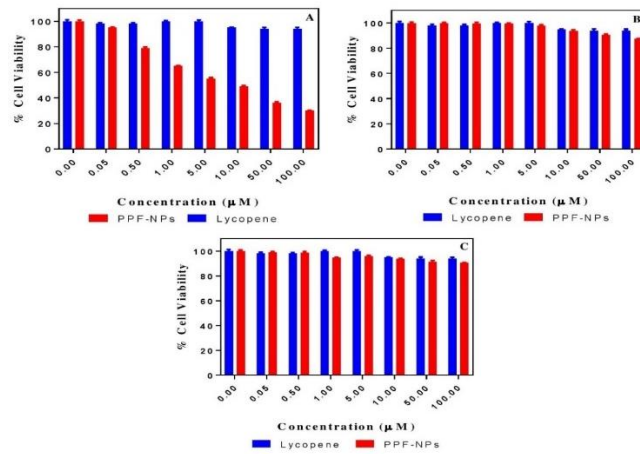


**Figure 5.** Results of MTT assay indicating the cell viability (%), (A) MCF-7 cells; (B) MCF-10A cells; (C) WB cells.

**Table 2.** Calculated LD<sub>50</sub> values of free Lycopene and PPF-NPs in various cell lines.

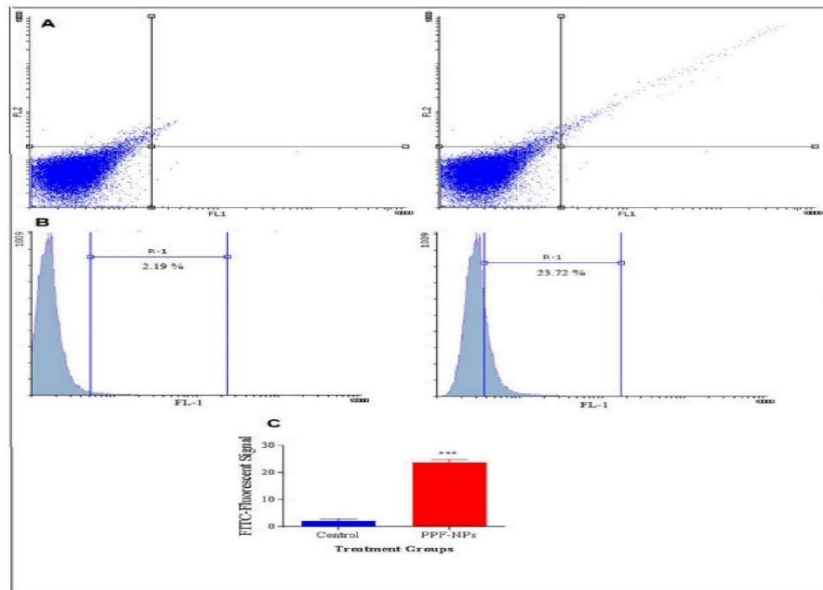
Cell line	Cell type	Formulation	LD <sub>50</sub> (μM)
MCF-7	A luminal breast cancer cell line	Free Lycopene	9.16
		PPF-NPs	3.09
MCF-10A	Normal breast cells	Free Lycopene	196.96
		PPF-NPs	482.19
WBCs	Normal white blood cell	Free Lycopene	199.82
		PPF-NPs	523.03

Table 2 emphasizes that the presence of folate as a carrier ligand of PPF-NPs intensified the difference between the cytotoxicity effect in cancer and normal cells. This intensification is related to the enhanced uptake of PPF-NPs via folate-specific receptors (FR) that mediate active transport in breast cancer cells. Due to the higher rate of metabolism in cancer cells, the PPF-NPs uptake is also increased. As such, the folate-engineered PPF-NPs appear to be absorbed more strongly by cancer cells than normal cells. This justified the folate decoration of the NPs. It seems that folate makes targeting lycopene to tumor cells possible, leading to less toxic effects on non-cancerous cells.

On the other hand, lycopene, a naturally available carotenoid, is free of untoward effects, and the proposed dose of lycopene is far from any toxicity for normal cells to die. Therefore, it seems that the specificity generated by folate targeting makes the PPF-NPs a suitable candidate to be used in chemotherapy. It revealed that the uptakes of PPF-NPs by cancer cells are somehow specific; therefore, it could be an excellent candidate to be used in chemotherapy.

### 3.1.4. Uptake of PPF-NPs by MCF7cells.

As shown in Figure 6A, the cells incubated with FITC-labeled PPF-NPs exhibited 23.72 % fluorescent intensity, while untreated control cells did not show any FITC-fluorescent signal (RN1 = 2.19 %). The uptake rate of PPF-NPs was significantly ( $p < 0.05$ ) higher than control (Figure 6B) by MCF-7 cells.



**Figure 6.** Results of flow cytometry indicating the uptake of PPF-NPs into MCF7 cells. The comparison between uptake rates of FITC labeled PPF-NPs. The values are mean  $\pm$  SD. \*\*\*/\*\*\*\* Indicates the significant difference from the control.

Figure 6C shows that in the presence of folate, there is no difference between the uptake of PP-NPs and PPF-NPs by MCF-7 cells. However, when folate was eliminated from the medium, the uptake of PPF-NPs was increased compared to PP-NPs. It is documented that simple PLGA nanoparticles could cross the cell membrane without targeting agents. However, it is assumed that adding a folate agent on the surface of NPs would increase the uptake of NPs by FR-positive cells. The fluorescent imaging microscopy images demonstrated the effective uptake and internalization of FITC-labeled PPF-NPs (Figure 7).

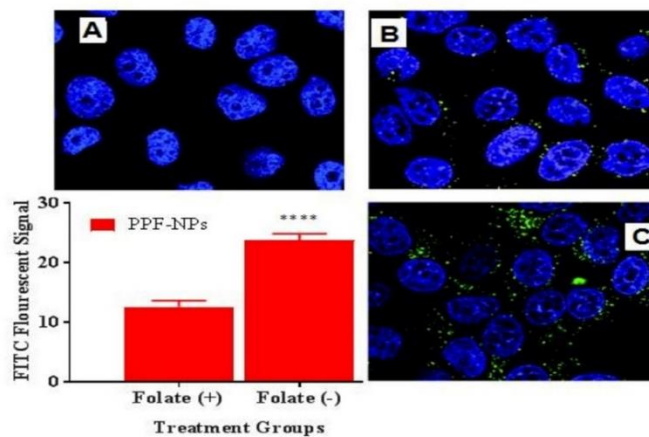


**Figure 7.** Results of fluorescent imaging microscopy showing the internalization of PPF-NPs into the MCF7 cells, where A, B, and C denote Control, PPF-NPs with folate, and PPF-NPs without folate, respectively.

The results showed higher internalization of PPF-NPs into the MCF7 cells in a folate-deficient media than in fortified media (Figure 7).

### 3.1.5. Apoptosis induction by NPs.

To confirm whether the reduced cell viability was due to apoptosis, acridine orange and ethidium bromide fluorescence staining was used to detect apoptotic cells. Using fluorescence microscopy, uniform normal green cells were observed in the control group (Figure 8A),

indicating viable cells, whereas an increased number of dark orange or red cells with increased PPF-NPs concentrations were detected (Figure 8B–D), indicating apoptotic cells.

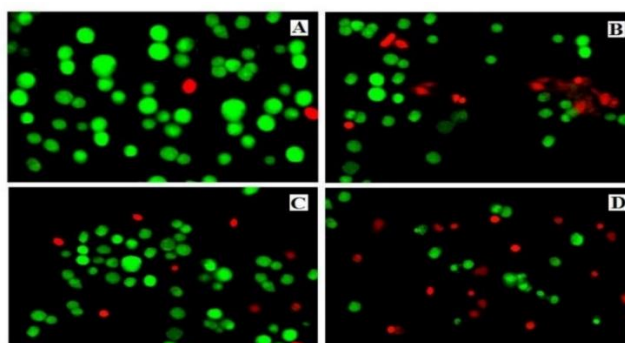


**Figure 8.** The results of the fluorescent imaging microscopy show the internalization of PPF-NPs into the MCF7 cells, where A denotes Control and B, C, and D denote PPF-NPs with increasing concentration, respectively.

Results are from three independent experiments. The cells treated with PPF-NPs showed an extended apoptosis relative to the control cells.

### 3.1.6. Acute and chronic toxicity.

No death or loss of body weight was detected in the studied animals. For the 100 mg/kg group, a reduction in serum glutamic-oxaloacetic transaminase (SGOT), an increase in serum glutamic-pyruvic transaminase (SGPT), a reduction in alkaline phosphatase (ALP) and direct bilirubin, increase in albumin and total protein, decrease in total leukocyte count were observed. Based on these results, the dose was decreased to 12.5, 6, and 3 mg/kg equivalent of lycopene. For 12.5 mg/kg, an increase in albumin and total protein and a decrease in total leukocyte count were detected. No abnormality in the other groups, i.e., 6 and 3 mg/kg equivalent of lycopene, were observed (Table 3).

**Table 3.** Acute toxicity of PPF-NPs in different concentrations (Control, 3, 6, 12.5, and 100 mg/kg equivalent of lycopene) on hematological markers in mice.

Parameter	Groups				
	Control	PPF-NPs (3 mg/kg)	PPF-NPs (6 mg/kg)	PPF-NPs (12.5 mg/kg)	PPF-NPs (100 mg/kg)
Animal weight (g)	20.4 ± 1.9	20.7 ± 2.7	19.5 ± 3.1	20.8 ± 2.7	21.3 ± 1.9
Urea (mg/dL)	61.4 ± 6.7	73.1 ± 0.8	61.4 ± 9.5	63.1 ± 7.8	62.6 ± 7.3
Cr (mg/dL)	0.49 ± 0.1	0.49 ± 0.1	0.51 ± 0.0	0.5 ± 0.1	0.50 ± 0.1
ALP (U/L)	492.6 ± 94.8	388.4 ± 97.6	375.2 ± 91.6	486.0 ± 91.9	232.4 ± 41.1 *
SGOT (U/L)	350.5 ± 123.6	360.2 ± 61.8	253.8 ± 8.7	354.0 ± 147.4 *	59.7 ± 8.3 *
SGPT (U/L)	36.6 ± 15.8	58.3 ± 12.1	48.2 ± 9.7	60.2 ± 6.2	79.5 ± 6.7 *
D. BIL (mg/dL)	0.48 ± 0.28	0.47 ± 0.1	0.48 ± 0.3	0.48 ± 0.0	0.27 ± 0.1 *
ALB (mg/dL)	2.1 ± 0.1	3.0 ± 0.5	3.1 ± 0.5	4.7 ± 0.2 *	4.4 ± 0.5 *
Total protein (mg/dL)	4.7 ± 0.6	4.4 ± 0.2	4.2 ± 1.3	6.8 ± 0.2 *	6.5 ± 0.4 *
Glucose (mg/dL)	182.3 ± 64.6	251.5 ± 98.2	243.0 ± 88.9	231.0 ± 19.8	161.0 ± 29.1
WBC (1000/mm <sup>3</sup> )	11.9 ± 2.8	10.8 ± 0.7	11.7 ± 0.7	4.6 ± 0.6 *	3.1 ± 0.1 *
RBC (Millin/mm <sup>3</sup> )	9.2 ± 0.2	8.9 ± 0.8	8.6 ± 0.4	8.3 ± 0.3	9.2 ± 0.4
HGB (mg/dL)	14.5 ± 0.3	12.8 ± 0.9	12.1 ± 0.8	12.4 ± 0.7	13.8 ± 0.8
Plt (1000/mm <sup>3</sup> )	1015.0 ± 76.7	655.0 ± 117.6	766.4 ± 61.5	987.8 ± 124.8 *	779.5 ± 62.1 *

The values are mean ± SD \*  $p < 0.05$  compared to control.

Therefore, the initial dose for the chronic toxicity test was chosen as 6, 3, 1.5, and 0.75 mg/kg equivalent of Lycopene from PPF-NPs. To investigate the chronic toxicity of blank NPs (PPF-NPs), the same amount of PPF-NPs (6 mg/kg equivalent of lycopene) was injected into

the control group. The results showed no significant hematological abnormality in any of the animal groups (Table 4).

**Table 4.** Chronic toxicity of PPF-NPs in different concentrations (control, 0.75, 1.5, 3, and 6 mg/kg equivalent of lycopene) on hematological markers in mice.

Parameter	Groups				
	Control	PPF-NPs (3 mg/kg)	PPF-NPs (6 mg/kg)	PPF-NPs (12.5 mg/kg)	PPF-NPs (100 mg/kg)
Animal weight (g)	20.6 ± 1.6	21.5 ± 2.1	20.3 ± 1.5	21.5 ± 1.4	19.4 ± 2.6
Urea (mg/dL)	62.3 ± 2.1	69.7 ± 10.7	71.2 ± 10.6	72.6 ± 13.2	71.0 ± 0.8
Cr (mg/dL)	0.48 ± 0.0	0.5 ± 0.1	0.5 ± 0.0	0.49 ± 0.1	0.5 ± 0.0
ALP (U/L)	495.0 ± 122.0	457.5 ± 83.6	456.4 ± 41.8	440.5 ± 122.3	424.3 ± 66.5
SGOT (U/L)	482.5 ± 98.0	490.0 ± 152.2	481.0 ± 76.7	494.0 ± 92.3	407.6 ± 3.5
SGPT (U/L)	63.5 ± 21.6	65.3 ± 32.5	76.6 ± 12.1	71.2 ± 17.8	54.5 ± 10.5
D. BIL (mg/dL)	0.58 ± 0.1	0.57 ± 0.0	0.50 ± 0.1	0.42 ± 0.1	0.5 ± 0.3
ALB (mg/dL)	2.0 ± 0.2	2.0 ± 0.4	1.97 ± 0.4	1.9 ± 0.3	2.4 ± 0.7
Total protein (mg/dL)	5.9 ± 1.9	4.9 ± 0.4	5.5 ± 0.7	5.1 ± 0.6	5.6 ± 1.1
Glucose (mg/dL)	210.3 ± 56.5	205.0 ± 80.3	187.7 ± 35.8	212.2 ± 7.2	205.0 ± 74.9
WBC (1000/mm <sup>3</sup> )	5.8 ± 0.1	6.9 ± 1.2	6.7 ± 1.5	6.6 ± 0.7	3.1 ± 5.4
RBC (Millin/mm <sup>3</sup> )	7.2 ± 0.3	7.7 ± 0.6	7.9 ± 0.2	7.6 ± 0.1	7.1 ± 0.5
HGB (mg/dL)	11.9 ± 0.4	11.3 ± 0.5	11.6 ± 0.7	11.2 ± 0.7	11.1 ± 0.8
Plt (1000/mm <sup>3</sup> )	1012 ± 214.6	927 ± 201	998 ± 161	1071 ± 277	870 ± 48.6

The values are mean ± SD \*  $p < 0.05$  compared to control.

### 3.1.7. *In vivo* prophylactic and anticancer activity: inhibition of tumor growth in rat model.

In spite of several rewarding properties of nanocarriers in cancer therapeutics, the curative efficacy was determined by investigating the prophylactic anticancer activity, tumor proliferation, and survival rate of the animal after administration of Lycopene and PPF-NPs in NMU-induced breast cancer animal model (Figure 9A–C).

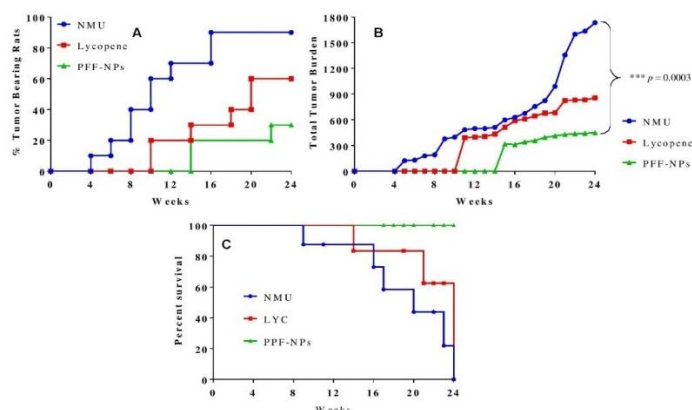


**Figure 9.** Prophylactic and anticancer activity of free Lycopene and PPF-NPs on NMU-induced breast cancer model: (A) % Tumor-bearing animals; (B) Total tumor burden; (C) Survival of animals upon 24 weeks of treatment where  $n=10$ ; and  $p<0.05$ .

The prophylactic and anticancer activity of lycopene was estimated by observing the survival of tumor-bearing animals, tumor latency, and tumor progression. Figure 9A illustrates tumor progression and animal survival after intravenous administration of Lycopene and PPF-NPs. After 4 weeks of treatment, there was the induction of tumors in animals of the control group (administered NMU only). However, it was observed that free Lycopene and PPF-NPs demonstrated noticeable effects after 10 and 14 weeks, respectively, indicating the potential prophylactic antitumor potential of lycopene. Moreover, after 16 weeks of NMU dose, almost all the animals in the control group developed tumors.

On the other hand, following 24 weeks, animals administered with concurrent Lycopene and PPF-NPs treatment showed nearly ~60% and ~30% tumor development in animals. The prophylactic and anticancer activity was thus revealed by delay in induction and progression of the tumor on antioxidant treatment. In brief, animals administered with antioxidant treatment (until 24 weeks) had tumor development at a slower rate than those in the treated (control) group. In addition, when evaluated against plain Lycopene (Figure 7B), the prophylactic antitumor potential of PPF-NPs was significantly higher ( $p < 0.001$ ). This observation could be due to the encapsulation of the drug lycopene within the nanocarrier. When the tumor burden was measured following 24 weeks of NMU administration, there were ~2.03-folds and ~3.86-folds lesser with lycopene ( $855.74 \pm 66.4 \text{ mm}^2$ ) and PPF-NPs ( $448.98 \pm 53.4 \text{ mm}^2$ ) administered animals, respectively, in comparison to NMU treated groups ( $1734.0 \pm 93.5 \text{ mm}^2$ ). Additionally, the effectiveness of lycopene on animal survival rate was observed by the Kaplan–Meier survival plot following 24 weeks of treatment regimen. The PPF-NPs showed the maximum prophylactic and better animal survival among all the treatments (Figure 9B and C). The PPF-NPs had subsisted considerable ( $P < 0.001$ ) progress in animal survival (100%) as compared to animals of free lycopene (62.5%) and negative control group (21.88%).

### 3.1.8. Tumor histology.

The control group rats exhibited adenocarcinomas (Figure 10). Cellular tumor lesions were observed with epithelial and stromal proliferation. The developed tumors were adenomatous and closely resembled florid sclerosing adenosis.

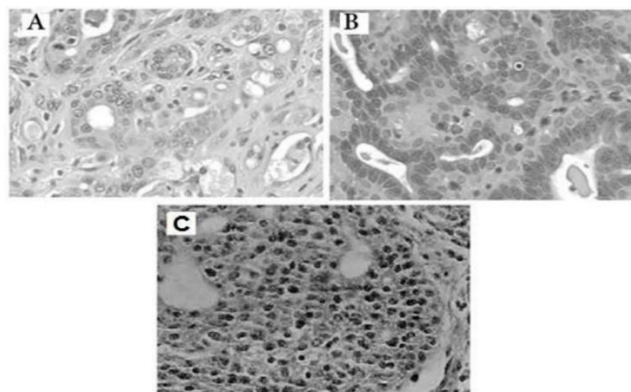


**Figure 10.** The inhibition of breast cancer tumor growth in rats using i.v. Injection of (A) blank NPs as control; (B) Lycopene; (C) PPF-NPs. The histopathological photomicrographs were taken upon H & E staining (hematoxylin and eosin) of tumors from control, lycopene, and PPF-NPs injection groups with 200 times magnification.

Carcinoma cells were found to be confined to the breast lobules and indicated a low-grade ductal carcinoma *in situ*. Atypical mitotic figures, along with increased mitotic index, moderate to severe cytologic atypia, jagged infiltrating margins, and coagulative tumor cell necrosis, exhibited diagnostic features of adenocarcinoma. More prominent angiogenesis was observed in the treated rats. Treated groups of rats demonstrated adenomas (Figure 10) with moderately cellular lesions consisting of stromal and epithelial components. The cellular architecture indicated fibroadenoma with fibro-epithelial lesion. A low mitotic index and mild to moderate cytologic atypia in the epithelial cells were indicative of fibroadenoma.

### 3.1.9. *In vivo* pharmacokinetic study.

The pharmacokinetic parameters of the formulation were estimated from the plasma profile vs time graph, as shown in Figure 4. *In vivo* plasma profile demonstrated improved bioavailability of lycopene when administered through PPF-NPs (Figure 4). Results demonstrated that  $t_{1/2}$  of free lycopene was less (14.21 hours) than that of PPF-NPs, with  $t_{1/2}$  of 22.67 hours, indicating the distribution of drugs to cancer cells via the targeting ligand. The half-life of PPF-NPs was significantly increased as compared to free lycopene at the same time max. The MRT of Lycopene received through PPF-NPs nanoparticles was higher than that of free Lycopene (Table 5). Significant differences between free Lycopene and PPF-NPs in terms of MRT were observed. Similarly, the AUC of Lycopene delivered through the PPF-NPs was found to be higher when compared to free Lycopene (Table 5).

**Table 5.** Calculated pharmacokinetic parameters.

Pharmacokinetics parameters	Lycopene Formulation Pharmacokinetics parameters after IV administration	
	Free Lycopene	PPF-NPs
AUC <sub>0-∞</sub> (ng h/ml)	17042.40	24110.64
MRT 0-∞ (h)	18.37	30.97
C <sub>max</sub> (ng/ml)	186.5	198.6
T <sub>max</sub> (h)	0.25	0.25
T <sub>1/2</sub>	14.21	22.67

The results demonstrated an improved bioavailability profile of the PPF-NPs, which further increases the probability of higher site-specific distribution due to the incorporation of the targeting ligand. These observations indicated the improved residing time of PPF-NPs in circulation and voted for the significance of the nanocarrier system by controlling the drug diffusion rate. Moreover, the improved bioavailability of PPF-NPs suggests significant localization of lycopene in the tumor cells via enhanced permeation and retention (EPR) effect.

### 3.2. Discussion.

Physiochemical properties like size and morphology primely enhance drug delivery efficiency at the tumor site. Dripping vessels with a gap size of 220 nm to 1.2 μm between adjacent endothelial cells are visualized in solid tumors due to deformities such as lack of pericytes and aberrant basement membrane formation. As a result, NPs with a size of 220 nm or smaller become accessible to tumors with higher retention time than normal tissues [64–68] by the EPR effect. For delivery into solid tumors, particle size in the range of 10–220 nm is inevitable as particle sizes of <10 nm are prone to faster renal clearance, whereas particle size of >220 nm may minimize the possibility of the NPs passing through the leaky vasculature system. Larger NPs in the range of 500 nm to μm are susceptible to phagocytic uptake and reticuloendothelial system (RES) for rapid elimination from blood [69–71]. Incorporation of targeting ligands may facilitate slight variations; as seen in the present study, PPF-NPs are in the size range of 293.1 nm as compared to 136.3 nm for PLGA formulation and 236.9 nm for PLGA-PEG formulation previously prepared and studied. The larger size of PPF-NPs compared to PLGA NPs and PLGA-PEG NPs might be because of the outside orientation of the PEG-folate moieties on the surface of NPs. Additionally, the larger size has maximized its drug content and encapsulation efficiency. This finding is similar to previous reports by other investigators [44,55]. A cellular uptake mechanism study in MCF-7 cells revealed that PPF-NPs have far greater uptakes by MCF-7 cells than free lycopene. This is particularly because MCF-7 is a folate receptor-positive cell line that expresses the folate receptor on its surface at

a significant level. The possibility of involving a receptor-mediated endocytosis mechanism increases the uptake of PPF-NPs. While its expression is limited in healthy tissues and organs, folate receptors are highly expressed in epithelial, ovarian, cervical, breast, lung, kidney, colorectal, and brain tumors [72,73]. Approximately 30 % of breast cancers and 80 % of stage IV metastatic triple-negative breast cancer (TNBC) tumors express folate receptors [74]. Therefore, the rationality of employing folic acid as a targeting ligand, a small, stable, inexpensive, and non-immunogenic molecule, is justified. As PPF-NPs have higher cytotoxicity in MCF-7 cells compared to MCF-10A and WBC cells, apparently, it has a higher capability of apoptosis in breast cancer cells (MCF-7). Previous investigations suggested that fewer PPF-NPs are required for apoptosis induction for an equal amount of lycopene. This indicates that PPF-NPs could effectively deliver Lycopene into MCF-7 cells and induce apoptosis. Free lycopene had lesser cytotoxicity in MCF-7 cells, significantly less than free lycopene. The cytotoxicity is obviously not due to these FDA-approved biocompatible polymers nor to the PVA used as an emulsifier in the NP preparation process, which remains in the NPs. The key mechanism that enhanced the cytotoxicity is the internalization of lycopene into cells by folate receptor-mediated endocytosis due to the presence of the targeting ligand folic acid. Due to increased cellular internalization of PPF-NPs, higher cellular uptake of the entrapped lycopene was enabled, along with their capability to escape the effect of P-gp pumps. Subsequently, PPF-NPs may play the role of intracellular drug reservoir that can gradually release the encapsulated drug into cellular cytoplasm and increase its therapeutic efficiency. In our investigation, we have selected a rat model where MNU induces a mammary tumor in the Sprague–Dawley rat. The rationality of using the rat model was due to the resemblance of the histologic structure of mammary gland tumors with that of human mammary tumors. This method of induction of mammary carcinomas by MNU in female rats is one of the most popular animal models for investigating breast carcinogenesis and mammary tumor treatment. Rat mammary tumors are predominantly ductal, similar to those of humans. Additionally, the MNU model has numerous benefits, including the reliability of tumor induction, organ site specificity, tumor of ductal origin and predominantly carcinomatous histopathologic characterization, and the ability to examine tumor initiation and promotion processes. In general, MNU-induced mammary carcinomas are aggressive and locally invasive. The present study revealed remarkable inhibition of mammary tumor incidence and multiplicity in Sprague–Dawley female rats with Lycopene-encapsulated PPF-NPs. The decreased growth of MNU-induced mammary tumors and tumor burden was noted in the rats treated with Lycopene-encapsulated NPs compared to the control group rats. It was also observed that several tumors in the rats of the control group were not only but also had characteristics diagnostic of adenocarcinoma, including increased mitotic index and prominent angiogenesis as compared to control. Even though the precise mechanism of reduced tumor size in tumor-bearing rats could not be elucidated in the present study, these findings are in accordant with our *in vitro* studies that demonstrated significant % inhibition in MTT study in human breast cancer cell lines MCF-7. The prophylactic and anticancer activity was established by delay in induction and progression of tumor on PPF-NPs treatment. There was a marked reduction in tumor incidence and burden, suggesting the efficient tumor growth inhibition produced by PPF-NPs. This could be associated with the intensification of PPF-NPs into tumors and the prohibition of fast drug degradation from the bloodstream [75]. The incidence, as well as the growth, of MNU-induced mammary tumors was profoundly minimized by Lycopene-encapsulated PPF-NPs. The Kaplan-Meier survival plot further demonstrated the greater and

significant survival of the MNU-treated animals upon treatment with PPF-NPs. Supposing clinical trials are imperative to estimate the antitumor ability of the tested NPs on cancer patients; the results of this study proposed strong potential for its use as a prophylactic as well as a therapeutic regimen for preventing and retarding breast cancer development. In view of the formidable effects of lycopene against cancer cells, its vigorous antiquity of being sound endurance within the human body, and its cost-effectiveness and availability in the market compared to other chemotherapy agents, it is contemplated that encapsulation of lycopene into folate-receptor-targeted PPF-NPs could present a contrivance for rendering this drug into clinical cancer therapeutics.

#### **4. Conclusions**

The present research suggests that delivery of lycopene into breast cancer cells via folate-receptor-targeted poly (lactide-co-glycolide) (PLGA)-polyethylene glycol (PEG) nanoparticles (NPs) can be grounded as a solid platform for efficient delivery this natural anticancer drug which otherwise has underprivileged physicochemical properties like low aqueous solubility and poor oral bioavailability. The only alternative that remained in the hands of the researchers to overcome this challenge is to maximize its delivery via an effective delivery system. Polymeric nanoparticulate drug delivery systems incorporating targeting ligands can prove to be a big smash. Hence, the present attempt to fabricate and evaluate the same was inveterate. As per the evaluation, the triple conjugate system (PPF) was fabricated, and NPs were prepared adequately. The results of the evaluated parameters of the NPs viz the release pattern, toxicity, and cytotoxicity reinforced the declaration. Results revealed that Folate-receptor-targeted NPs are more efficient for cellular internalization and cell proliferation inhibition than free lycopene, and it can be concluded that the delivery system is capable of this.

Additionally, the cell cytotoxicity study performed in MCF-7, MCF-10A, and WB cells, as well as flow cytometry and fluorescence imaging, confirm the fruitful internalization of NPs. Acute and chronic toxicity tests showed when administered intravenously, the extent of lycopene equivalent of NPs for a considerable decrease in the breast cancer tumor growth rate is 6 mg/kg. The fabricated delivery system of NPs exhibited substantial *In vivo* prophylactic and anticancer activity in the tumor model. Furthermore, the mechanism of cell death (Apoptosis) studied in MCF-7 cells and *In vivo* prophylactic and anticancer activity using an MNU-induced rat tumor model demonstrated via Kaplan–Meier survival plot reassure a bright gateway suggestive to clinical study.

#### **Funding**

This research received no external funding.

#### **Acknowledgments**

The authors acknowledge Alpha Remedies, Ambala, India, for providing lycopene as a kind gift.

#### **Conflicts of Interest**

The authors declare no conflict of interest.

## References

1. Pedersen, S.F.; Stock, C. Ion Channels and Transporters in Cancer: Pathophysiology, Regulation, and Clinical Potential. *Cancer Res.* **2013**, *73*, 1658–1661, <https://doi.org/10.1158/0008-5472.CAN-12-4188>.
2. Nelson, E.R.; Chang, C.-Y.; McDonnell, D.P. Cholesterol and breast cancer pathophysiology. *Trends Endocrinol. Metab.* **2014**, *25*, 649–655, <https://doi.org/10.1016/j.tem.2014.10.001>.
3. Anand, U.; Dey, A.; Chandel, A.K.S.; Sanyal, R.; Mishra, A.; Pandey, D.K.; De Falco, V.; Upadhyay, A.; Kandimalla, R.; Chaudhary, A.; Dhanjal, J.K.; Dewanjee, S.; Vallamkondu, J.; Pérez de la Lastra, J.M. Cancer chemotherapy and beyond: Current status, drug candidates, associated risks and progress in targeted therapeutics. *Genes Dis.* **2023**, *10*, 1367–1401, <https://doi.org/10.1016/j.gendis.2022.02.007>.
4. Alshareeda, A.T.; Nur Khatijah, M.Z.; Al-Sowayan, B.S. Nanotechnology: A revolutionary approach to prevent breast cancer recurrence. *Asian J. Surg.* **2023**, *46*, 13–17, <https://doi.org/10.1016/j.asjsur.2022.03.002>.
5. Mehra, N.K.; Gulbake, A. Micro- and Nanotechnologies-Based Product Development, 1<sup>st</sup> Edition; Mehra, N.K., Gulbake, A., Eds.; CRC Press, Boca Raton, **2021**; 1-326, <https://doi.org/10.1201/9781003043164>.
6. Kapała, A.; Szlendak, M.; Motacka, E. The Anticancer Activity of Lycopene: A Systematic Review of Human and Animal Studies. *Nutrients* **2022**, *14*, 5152, <https://doi.org/10.3390/nu14235152>.
7. Anand, S.; Bharadvaja, N. Potential Benefits of Nutraceuticals for Oxidative Stress Management. *Rev. Bras. Farmacogn.* **2022**, *32*, 211–220, <https://doi.org/10.1007/s43450-022-00246-w>.
8. Maiuolo, J.; Gliozzi, M.; Carresi, C.; Musolino, V.; Oppedisano, F.; Scarano, F.; Nucera, S.; Scicchitano, M.; Bosco, F.; Macri, R.; Ruga, S.; Cardamone, A.; Coppoletta, A.; Mollace, A.; Cognetti, F.; Mollace, V. Nutraceuticals and Cancer: Potential for Natural Polyphenols. *Nutrients* **2021**, *13*, 3834, <https://doi.org/10.3390/nu13113834>.
9. Chu, M.; Zheng, C.; Chen, C.; Song, G.; Hu, X.; Wang, Z.-W. Targeting cancer stem cells by nutraceuticals for cancer therapy. *Semin. Cancer Biol.* **2022**, *85*, 234–245, <https://doi.org/10.1016/j.semcancer.2021.07.008>.
10. Fayeze, S.; Ayoub, I.M.; Mostafa, N.M.; Moussa, A.Y.; Gamal ElDin, M.I.; El-Shazly, M. Nutraceuticals in Cancer Therapy. In *Handbook of Oxidative Stress in Cancer: Therapeutic Aspects*; Chakraborti, S., Ed.; Springer, Singapore, **2022**; 189-208, [https://doi.org/10.1007/978-981-16-5422-0\\_15](https://doi.org/10.1007/978-981-16-5422-0_15).
11. Katerji, M.; Filippova, M.; Duerksen-Hughes, P. Approaches and Methods to Measure Oxidative Stress in Clinical Samples: Research Applications in the Cancer Field. *Oxid. Med. Cell. Longev.* **2019**, *2019*, 1279250, <https://doi.org/10.1155/2019/1279250>.
12. Barrera, G.; Cucci, M.A.; Grattarola, M.; Dianzani, C.; Muzio, G.; Pizzimenti, S. Control of Oxidative Stress in Cancer Chemoresistance: Spotlight on Nrf2 Role. *Antioxidants* **2021**, *10*, 510, <https://doi.org/10.3390/antiox10040510>.
13. Almeida, T.P.; Ramos, A.A.; Ferreira, J.; Azqueta, A.; Rocha, E. Bioactive Compounds from Seaweed with Anti-Leukemic Activity: A Mini-Review on Carotenoids and Phlorotannins. *Mini-Rev. Med. Chem.* **2020**, *20*, 39–53, <https://doi.org/10.2174/1389557519666190311095655>.
14. James, A.S.; Ugbaja, R.N.; Ugwor, E.I.; Thomas, F.C.; Akamo, A.J.; Akinloye, D.I.; Eteng, O.E.; Salami, S.K.; Emmanuel, E.A.; Ugbaja, V.C. Lycopene abolishes palmitate-mediated myocardial inflammation in female Wistar rats via modulation of lipid metabolism, NF- $\kappa$ B signalling pathway, and augmenting the antioxidant systems. *Nutr., Metab. Cardiovasc. Dis.* **2023**, *33*, 671–681, <https://doi.org/10.1016/j.numecd.2022.11.026>.
15. Assar, E.A.; Vidalle, M.C.; Chopra, M.; Hafizi, S. Lycopene acts through inhibition of I $\kappa$ B kinase to suppress NF- $\kappa$ B signaling in human prostate and breast cancer cells. *Tumor Biol.* **2016**, *37*, 9375–9385, <https://doi.org/10.1007/s13277-016-4798-3>.
16. Polinati, R.M.; Teodoro, A.J.; Correa, M.G.; Casanova, F.A.; Passos, C.L.A.; Silva, J.L.; Fialho, E. Effects of lycopene from guava (*Psidium guajava* L.) derived products on breast cancer cells. *Nat. Prod. Res.* **2022**, *36*, 1405–1408, <https://doi.org/10.1080/14786419.2021.1880402>.
17. Song, X.; Luo, Y.; Ma, L.; Hu, X.; Simal-Gandara, J.; Wang, L.-S.; Bajpai, V.K.; Xiao, J.; Chen, F. Recent trends and advances in the epidemiology, synergism, and delivery system of lycopene as an anticancer agent. *Semin. Cancer Biol.* **2021**, *73*, 331–346, <https://doi.org/10.1016/j.semcancer.2021.03.028>.
18. Puah, B.-P.; Jalil, J.; Attiq, A.; Kamisah, Y. New Insights into Molecular Mechanism behind Anticancer Activities of Lycopene. *Molecules* **2021**, *26*, 3888, <https://doi.org/10.3390/molecules26133888>.

19. Bin-Jumah, M.N.; Nadeem, M.S.; Gilani, S.J.; Mubeen, B.; Ullah, I.; Alzarea, S.I.; Ghoneim, M.M.; Alshehri, S.; Al-Abbasi, F.A.; Kazmi, I. Lycopene: A Natural Arsenal in the War against Oxidative Stress and Cardiovascular Diseases. *Antioxidants* **2022**, *11*, 232, <https://doi.org/10.3390/antiox11020232>.
20. Przybylska, S.; Tokarczyk, G. Lycopene in the Prevention of Cardiovascular Diseases. *Int. J. Mol. Sci.* **2022**, *23*, 1957, <https://doi.org/10.3390/ijms23041957>.
21. Jain, A.; Sharma, G.; Ghoshal, G.; Kesharwani, P.; Singh, B.; Shivhare, U.S.; Katare, O.P. Lycopene loaded whey protein isolate nanoparticles: An innovative endeavor for enhanced bioavailability of lycopene and anticancer activity. *Int. J. Pharm.* **2018**, *546*, 97–105, <https://doi.org/10.1016/j.ijpharm.2018.04.061>.
22. Faisal, W.; O'Driscoll, C.M.; Griffin, B.T. Bioavailability of lycopene in the rat: the role of intestinal lymphatic transport. *J. Pharm. Pharmacol.* **2010**, *62*, 323–331, <https://doi.org/10.1211/jpp.62.03.0006>.
23. Falsafi, S.R.; Rostamabadi, H.; Babazadeh, A.; Tarhan, Ö.; Rashidinejad, A.; Boostani, S.; Khoshnoudi-Nia, S.; Akbari-Alavijeh, S.; Shaddel, R.; Jafari, S.M. Lycopene nanodelivery systems; recent advances. *Trends Food Sci. Technol.* **2022**, *119*, 378–399, <https://doi.org/10.1016/j.tifs.2021.12.016>.
24. Iqbal, J.; Anwar, F.; Afridi, S. Targeted Drug Delivery Systems and Their Therapeutic Applications in Cancer and Immune Pathological Conditions. *Infect. Disord. Drug Targets* **2017**, *17*, 149–159, <https://doi.org/10.2174/1871526517666170606102623>.
25. Ma, Y.; Zhong, L.; Peng, Z.; Liu, X.; Ouyang, D.; Guan, S. Development of a Highly Water-Soluble Lycopene Cyclodextrin Ternary Formulation by the Integrated Experimental and Modeling Techniques. *AAPS PharmSciTech* **2021**, *22*, 5, <https://doi.org/10.1208/s12249-020-01861-3>.
26. Kalyane, D.; Raval, N.; Maheshwari, R.; Tambe, V.; Kalia, K.; Tekade, R.K. Employment of enhanced permeability and retention effect (EPR): Nanoparticle-based precision tools for targeting of therapeutic and diagnostic agent in cancer. *Mater. Sci. Eng. C* **2019**, *98*, 1252–1276, <https://doi.org/10.1016/j.msec.2019.01.066>.
27. Taylor, J.; Bebawy, M. Proteins Regulating Microvesicle Biogenesis and Multidrug Resistance in Cancer. *Proteomics* **2019**, *19*, 1800165, <https://doi.org/10.1002/pmic.201800165>.
28. Li, C.; Guan, X.; Xue, H.; Wang, P.; Wang, M.; Gai, X. Reversal of P-glycoprotein-mediated multidrug resistance is induced by saikosaponin D in breast cancer MCF-7/adriamycin cells. *Pathol. Res. Pract.* **2017**, *213*, 848–853, <https://doi.org/10.1016/j.prp.2017.01.022>.
29. Halder, J.; Pradhan, D.; Kar, B.; Ghosh, G.; Rath, G. Nanotherapeutics approaches to overcome P-glycoprotein-mediated multidrug resistance in cancer. *Nanomedicine* **2022**, *40*, 102494, <https://doi.org/10.1016/j.nano.2021.102494>.
30. Riley, R.S.; June, C.H.; Langer, R.; Mitchell, M.J. Delivery technologies for cancer immunotherapy. *Nat. Rev. Drug Discov.* **2019**, *18*, 175–196, <https://doi.org/10.1038/s41573-018-0006-z>.
31. Hussain, Z.; Khan, S.; Imran, M.; Sohail, M.; Shah, S.W.A.; de Matas, M. PEGylation: a promising strategy to overcome challenges to cancer-targeted nanomedicines: a review of challenges to clinical transition and promising resolution. *Drug Deliv. Transl. Res.* **2019**, *9*, 721–734, <https://doi.org/10.1007/s13346-019-00631-4>.
32. Kim, J.W.; Cochran, J.R. Targeting ligand–receptor interactions for development of cancer therapeutics. *Curr. Opin. Chem. Biol.* **2017**, *38*, 62–69, <https://doi.org/10.1016/j.cbpa.2017.03.010>.
33. David, L.L.; Daniels, A.; Habib, S.; Singh, M. Gold nanoparticles in transferrin-targeted dual-drug delivery *in vitro*. *J. Drug Deliv. Sci. Technol.* **2023**, *90*, 105168, <https://doi.org/10.1016/j.jddst.2023.105168>.
34. Srinivasarao, M.; Low, P.S. Ligand-Targeted Drug Delivery. *Chem. Rev.* **2017**, *117*, 12133–12164, <https://doi.org/10.1021/acs.chemrev.7b00013>.
35. Shams, A.; Shabani, R.; Asgari, H.; Karimi, M.; Najafi, M.; Asghari-Jafarabadi, M.; Razavi, S.M.; Miri, S.R.; Abbasi, M.; Mohammadi, A.; Kuruji, M. *In vitro* elimination of EL4 cancer cells from spermatogonia stem cells by miRNA-143- and 206-loaded folic acid-conjugated PLGA nanoparticles. *Nanomedicine* **2022**, *17*, 531–545, <https://doi.org/10.2217/nmm-2021-0210>.
36. Biffi, S.; Voltan, R.; Bortot, B.; Zauli, G.; Secchiero, P. Actively targeted nanocarriers for drug delivery to cancer cells. *Expert Opin. Drug Deliv.* **2019**, *16*, 481–496, <https://doi.org/10.1080/17425247.2019.1604679>.
37. Farran, B.; Pavitra, E.; Kasa, P.; Peela, S.; Rama Raju, G.S.; Nagaraju, G.P. Folate-targeted immunotherapies: Passive and active strategies for cancer. *Cytokine Growth Factor Rev.* **2019**, *45*, 45–52, <https://doi.org/10.1016/j.cytogfr.2019.02.001>.
38. Zamani, M.; Aghajanzadeh, M.; Sharafi, A.; Rostamizadeh, K.; Danafar, H. Targeted drug delivery via folate decorated nanocarriers based on linear polymer for treatment of breast cancer. *Pharm. Dev. Technol.* **2022**, *27*, 19–24, <https://doi.org/10.1080/10837450.2021.2018457>.

39. Frigerio, B.; Bizzoni, C.; Jansen, G.; Leamon, C.P.; Peters, G.J.; Low, P.S.; Matherly, L.H.; Figini, M. Folate Folate receptors and transporters: biological role and diagnostic/therapeutic targets in cancer and other diseases. *J. Exp. Clin. Cancer Res.* **2019**, *38*, 125, <https://doi.org/10.1186/s13046-019-1123-1>.
40. Nguyen, V.D.; Min, H.-K.; Kim, C.-S.; Han, J.; Park, J.-O.; Choi, E. Folate receptor-targeted liposomal nanocomplex for effective synergistic photothermal-chemotherapy of breast cancer *In vivo*. *Colloids Surf. B Biointerfaces* **2019**, *173*, 539–548, <https://doi.org/10.1016/j.colsurfb.2018.10.013>.
41. Garizo, A.R.; Castro, F.; Martins, C.; Almeida, A.; Dias, T.P.; Fernandes, F.; Barrias, C.C.; Bernardes, N.; Fialho, A.M.; Sarmiento, B. p28-functionalized PLGA nanoparticles loaded with gefitinib reduce tumor burden and metastases formation on lung cancer. *J. Control. Release* **2021**, *337*, 329–342, <https://doi.org/10.1016/j.jconrel.2021.07.035>.
42. Zheng, Y.; Cantley, L.C. Toward a better understanding of folate metabolism in health and disease. *J. Exp. Med.* **2019**, *216*, 253–266, <https://doi.org/10.1084/jem.20181965>.
43. Yadav, B.; Chauhan, M.; Shekhar, S.; Kumar, A.; Mehata, A.K.; Nayak, A.K.; Dutt, R.; Garg, V.; Kailashiya, V.; Muthu, M.S.; Sonali; Singh, R.P. RGD-decorated PLGA nanoparticles improved effectiveness and safety of cisplatin for lung cancer therapy. *Int. J. Pharm.* **2023**, *633*, 122587, <https://doi.org/10.1016/j.ijpharm.2023.122587>.
44. Yadav, K.; Yadav, D.; Yadav, M.; Kumar, S. Noscipine Loaded PLGA Nanoparticles Prepared Using Oil-in-Water Emulsion Solvent Evaporation Method. *J. Nanopharm. Drug Deliv.* **2016**, *3*, 97–105, <https://doi.org/10.1166/jnd.2015.1074>.
45. McCall, R.L.; Sirianni, R.W. PLGA Nanoparticles Formed by Single- or Double-Emulsion with Vitamin E-TPGS. *J. Vis. Exp.* **2013**, *82*, e51015, <https://doi.org/10.3791/51015>.
46. Rocha, C.V.; Gonçalves, V.; da Silva, M.C.; Bañobre-López, M.; Gallo, J. PLGA-Based Composites for Various Biomedical Applications. *Int. J. Mol. Sci.* **2022**, *23*, 2034, <https://doi.org/10.3390/ijms23042034>.
47. Yeh, T.F.; Chen, C.M.; Wu, S.Y.; Husan, Z.; Li, T.C.; Hsieh, W.S.; Tsai, C.H.; Lin, H.C. Intratracheal Administration of Budesonide/Surfactant to Prevent Bronchopulmonary Dysplasia. *Am. J. Respir. Crit. Care Med.* **2016**, *193*, 86–95, <https://doi.org/10.1164/rccm.201505-0861OC>.
48. Rafiei, P.; Haddadi, A. Docetaxel-loaded PLGA and PLGA-PEG nanoparticles for intravenous application: pharmacokinetics and biodistribution profile. *Int. J. Nanomed.* **2017**, *12*, 935–947, <https://doi.org/10.2147/IJN.S121881>.
49. Rosca, I.D.; Watari, F.; Uo, M. Microparticle formation and its mechanism in single and double emulsion solvent evaporation. *J. Control. Release* **2004**, *99*, 271–280, <https://doi.org/10.1016/j.jconrel.2004.07.007>.
50. Das, P.J.; Paul, P.; Mukherjee, B.; Mazumder, B.; Mondal, L.; Baishya, R.; Debnath, M.C.; Dey, K.S. Pulmonary Delivery of Voriconazole Loaded Nanoparticles Providing a Prolonged Drug Level in Lungs: A Promise for Treating Fungal Infection. *Mol. Pharmaceutics* **2015**, *12*, 2651–2664, <https://doi.org/10.1021/acs.molpharmaceut.5b00064>.
51. Zhang, H.; Jiang, L.; Tong, M.; Lu, Y.; Ouyang, X.-K.; Ling, J. Encapsulation of curcumin using fucoidan stabilized zein nanoparticles: Preparation, characterization, and in vitro release performance. *J. Mol. Liq.* **2021**, *329*, 115586, <https://doi.org/10.1016/j.molliq.2021.115586>.
52. Cao, L.-B.; Zeng, S.; Zhao, W. Highly Stable PEGylated Poly(lactic-co-glycolic acid) (PLGA) Nanoparticles for the Effective Delivery of Docetaxel in Prostate Cancers. *Nanoscale Res. Lett.* **2016**, *11*, 305, <https://doi.org/10.1186/s11671-016-1509-3>.
53. Ahmed, S.; Kaur, K. Design, synthesis, and validation of an in vitro platform peptide-whole cell screening assay using MTT reagentFootnote. *J. Taibah Univ. Sci.* **2017**, *11*, 487–496, <https://doi.org/10.1016/j.jtusci.2016.10.001>.
54. Lupu, A.R.; Popescu, T. The noncellular reduction of MTT tetrazolium salt by TiO<sub>2</sub> nanoparticles and its implications for cytotoxicity assays. *Toxicol. in Vitro* **2013**, *27*, 1445–1450, <https://doi.org/10.1016/j.tiv.2013.03.006>.
55. Chen, J.; Li, S.; Shen, Q.; He, H.; Zhang, Y. Enhanced cellular uptake of folic acid–conjugated PLGA–PEG nanoparticles loaded with vincristine sulfate in human breast cancer. *Drug Dev. Ind. Pharm.* **2011**, *37*, 1339–1346, <https://doi.org/10.3109/03639045.2011.575162>.
56. Chelliah, R.; Oh, D.-H. Screening for Anticancer Activity: Dual Staining Method. In *Methods in Actinobacteriology*; Dharumadurai, D., Ed.; Humana, New York, NY, **2022**; 427–429, [https://doi.org/10.1007/978-1-0716-1728-1\\_55](https://doi.org/10.1007/978-1-0716-1728-1_55).

57. Yuet Ping, K.; Darah, I.; Chen, Y.; Sreeramanan, S.; Sasidharan, S. Acute and Subchronic Toxicity Study of *Euphorbia hirta* L. Methanol Extract in Rats. *BioMed Res. Int.* **2013**, *2013*, 182064, <https://doi.org/10.1155/2013/182064>.
58. OECD Guidelines for the Testing of Chemicals. Organization for Economic Development and Cooperation **1994**. Accessed 12 July 2018.
59. Waynforth, H.B.; Magee, P.N. The Effect of N-Nitroso-N-Methylurea and N-Dimethylnitrosamine on Cell Mediated and Humoral Immune Responses in Rats and Mice. *Br. J. Cancer* **1974**, *30*, 512–523, <https://doi.org/10.1038/bjc.1974.230>.
60. Gal, A.F.; Stan, L.; Tăbăran, F.; Rugină, D.; Cătoi, A.F.; Andrei, S. Chemopreventive Effects of Propolis in the MNU-Induced Rat Mammary Tumor Model. *Oxid. Med. Cell. Longev.* **2020**, *2020*, 4014838, <https://doi.org/10.1155/2020/4014838>.
61. El-Diasty, H.H.G.M.; El-Sayyad, H.; Refaat, S.; El-Ghaweet, H. Efficacy of Quercetin-Sensitized Cisplatin against N-Nitroso-NMethylurea Induced Testicular Carcinogenesis in Wistar Rats. *Asian Pac. J. Cancer Prev.* **2021**, *22*, 75–84, <https://doi.org/10.31557/APJCP.2021.22.1.75>.
62. Barba, A.I.O.; Hurtado, M.C.; Mata, M.C.S.; Ruiz, V.F.; de Tejada, M.L.S. Application of a UV–vis detection-HPLC method for a rapid determination of lycopene and  $\beta$ -carotene in vegetables. *Food Chem.* **2006**, *95*, 328–336, <https://doi.org/10.1016/j.foodchem.2005.02.028>.
63. Dolatabadi, S.; Karimi, M.; Nasirizadeh, S.; Hatamipour, M.; Golmohammadzadeh, S.; Jaafari, M.R. Preparation, characterization and *In vivo* pharmacokinetic evaluation of curcuminoids-loaded solid lipid nanoparticles (SLNs) and nanostructured lipid carriers (NLCs). *J. Drug Deliv. Sci. Technol.* **2021**, *62*, 102352, <https://doi.org/10.1016/j.jddst.2021.102352>.
64. Maeda, H. The enhanced permeability and retention (EPR) effect in tumor vasculature: the key role of tumor-selective macromolecular drug targeting. *Adv. Enzyme Regul.* **2001**, *41*, 189–207, [https://doi.org/10.1016/S0065-2571\(00\)00013-3](https://doi.org/10.1016/S0065-2571(00)00013-3).
65. Kang, H.; Rho, S.; Stiles, W.R.; Hu, S.; Baek, Y.; Hwang, D.W.; Kashiwagi, S.; Kim, M.S.; Choi, H.S. Size-Dependent EPR Effect of Polymeric Nanoparticles on Tumor Targeting. *Adv. Healthc. Mater.* **2020**, *9*, 1901223, <https://doi.org/10.1002/adhm.201901223>.
66. Singh, M.S.; Bhaskar, S. Nanocarrier-based immunotherapy in cancer management and research. *ImmunoTargets Ther.* **2014**, 121–134, <https://doi.org/10.2147/ITT.S62471>.
67. Pourgholi, A.; Dadashpour, M.; Mousapour, A.; Firouzi Amandi, A.; Zarghami, N. Anticancer Potential of Silibinin Loaded Polymeric Nanoparticles against Breast Cancer Cells: Insight into the Apoptotic Genes Targets. *Asian Pac. J. Cancer Prev.* **2021**, *22*, 2587–2596, <https://doi.org/10.31557/APJCP.2021.22.8.2587>.
68. Wu, J. The Enhanced Permeability and Retention (EPR) Effect: The Significance of the Concept and Methods to Enhance Its Application. *J. Pers. Med.* **2021**, *11*, 771, <https://doi.org/10.3390/jpm11080771>.
69. Maeda, H.; Wu, J.; Sawa, T.; Matsumura, Y.; Hori, K. Tumor vascular permeability and the EPR effect in macromolecular therapeutics: a review. *J. Control. Release* **2000**, *65*, 271–284, [https://doi.org/10.1016/S0168-3659\(99\)00248-5](https://doi.org/10.1016/S0168-3659(99)00248-5).
70. Roy, I.; Vij, N. Nanodelivery in airway diseases: Challenges and therapeutic applications. *Nanomed.: Nanotechnol. Biol. Med.* **2010**, *6*, 237–244, <https://doi.org/10.1016/j.nano.2009.07.001>.
71. Wang, R.; Zhang, Z.; Liu, B.; Xue, J.; Liu, F.; Tang, T.; Liu, W.; Feng, F.; Qu, W. Strategies for the design of nanoparticles: starting with long-circulating nanoparticles, from lab to clinic. *Biomater. Sci.* **2021**, *9*, 3621–3637, <https://doi.org/10.1039/D0BM02221G>.
72. McCord, E.; Pawar, S.; Koneru, T.; Tatiparti, K.; Sau, S.; Iyer, A.K. Folate Receptors' Expression in Gliomas May Possess Potential Nanoparticle-Based Drug Delivery Opportunities. *ACS Omega* **2021**, *6*, 4111–4118, <https://doi.org/10.1021/acsomega.0c05500>.
73. Varan, G.; Varan, C.; Erdoğan, N.; Bilensoy, E. Chapter 7 - Folate receptor-mediated targeted breast cancer nanomedicine. In *Targeted Nanomedicine for Breast Cancer Therapy*; Paliwal, S.R., Paliwal, R., Eds.; Academic Press, **2022**; 153–169, <https://doi.org/10.1016/B978-0-12-824476-0.00012-7>.
74. Necela, B.M.; Crozier, J.A.; Andorfer, C.A.; Lewis-Tuffin, L.; Kachergus, J.M.; Geiger, X.J.; Kalari, K.R.; Serie, D.J.; Sun, Z.; Aspita, A.M.; O'Shannessy, D.J.; Maltzman, J.D.; McCullough, A.E.; Pockaj, B.A.; Cunliffe, H.E.; Ballman, K.V.; Thompson, E.A.; Perez, E.A. Folate Receptor- $\alpha$  (FOLR1) Expression and Function in Triple Negative Tumors. *PLoS One* **2015**, *10*, e0122209, <https://doi.org/10.1371/journal.pone.0122209>.

75. Yi, Y.; Kim, J.H.; Kang, H.-W.; Oh, H.S.; Kim, S.W.; Seo, M.H. A Polymeric Nanoparticle Consisting of MPEG-PLA-Toco and PLMA-COONa as a Drug Carrier: Improvements in Cellular Uptake and Biodistribution. *Pharm. Res.* **2005**, *22*, 200–208, <https://doi.org/10.1007/s11095-004-1187-1>.